CHEMISTRY OF MATERIALS
Article

Chem. Mater. **2010,** *22,* 3735–3745 3735
DOI:10.1021/cm100798q

Structural−Property Relationship in Pyrazino[2,3-g]quinoxaline Derivatives: Morphology, Photophysical, and Waveguide Properties

Xiao Wang, Yan Zhou, Ting Lei, Nan Hu, Er-Qiang Chen,* and Jian Pei*

Beijing National Laboratory for Molecular Sciences, Key Laboratories of Bioorganic Chemistry and Molecular Engineering and of Polymer Chemistry and Physics of Ministry of Education, College of Chemistry and Molecular Engineering, Peking University, Beijing 100871, China

Received March 18, 2010. Revised Manuscript Received May 7, 2010

The objective of this contribution is to achieve crystalline one-dimensional organic micro/nanostructures by self-assembling for active waveguides and other optoelectronic nanodevices. To improve solid emitting performance for highly efficient waveguide fibers, our strategy here is to adopt nonplanar conjugated segments to minimize unfavorably intermolecular fluorescent quenching in solid state; meanwhile, long alkyl chains are added as structural group that controls molecular packing. With this intention, a series of molecules based on pyrazino[2,3-g]quinoxaline (**PyQ**) units were developed. The effects of the molecular geometry and symmetry on their optical properties, crystal dimensions, liquid crystals, and active waveguide properties were studied in detail to understand the structure−property relationship of organic conjugated molecules, which is of vital importance to rational design for organic self-assemblies toward optoelectronic applications. On a single molecular level, the molecular structures and their optical properties were correlated by computational methods. The combined results of morphology study, single crystal structure and two-dimensional wide-angle X-ray diffraction (2D-WAXD) indicated that the loss of the different molecular symmetry element affected the crystal dimensions. The microfibers of molecules **1** and **2** with their desirable crystal dimensions and surfaces were proved to be low-loss waveguide materials (0.02−0.05 dB/μm). Hence, we suggest that nonplanar aromatic core modified with proper side group may represent a promising approach to achieve crystalline optical waveguides. These structure−property investigations provide a deeper understanding for the structure and intermolecular interactions of such molecular aggregates.

Introduction

Because of their unique optical and electronic properties, organic conjugated molecules have been widely applied in dye industry,[1] fundamental electron/energy transfer studies,[2] biological fluorescent probes,[3] dye sensitized solar cells,[4] and information storage techniques (CD-R, DVD-R).[1,5] Recently, with the rapid developments of organic electronics[6] and nano-optics,[7] the micro/nano structure of such molecule aggregates have attracted considerable attentions because of their promising application in miniaturized optoelectronics, such as organic field-effect transistor,[8] chemical sensors,[9] optical waveguides and lasers.[10]

Organic materials as one-dimensional (1D) active waveguide with high efficiency are required to process good fluorescent emission, proper crystal dimensions, and smooth crystal surface.[10] However, for conventional organic semiconductors with flat aromatic cores, there is a dilemma. On the one hand, these molecules tend to form face-to-face stacking due to considerable $\pi-\pi$ interactions; however, such cofacial arrangement as H-aggregates does not

*Corresponding author. E-mail: jianpei@pku.edu.cn.

(1) Zollinger, H. *Color Chemistry: Syntheses, Properties and Applications of Organic Dyes and Pigments*, rev. ed.; Wiley-VCH: Zürich, Switzerland, 2003; Chapter 14.
(2) (a) Miller, J. R.; Calcaterra, L. T.; Closs, G. L. *J. Am. Chem. Soc.* **1984**, *106*, 3047–3049. (b) Marcus, R. A. *Pure Appl. Chem.* **1997**, *69*, 13–29.
(3) Zhang, J.; Campbell, R. E.; Ting, A. Y.; Tsien, R. Y. *Nat. Rev. Mol. Cell Biol.* **2002**, *3*, 906–918.
(4) (a) O' Regan, B.; Grätzel, M. *Nature* **1991**, *353*, 737–740. (b) Lee, K.; Park, S. W.; Ko, M. J.; Kim, K.; Park, N.-G. *Nat. Mater.* **2009**, *8*, 665–671.
(5) Shang, Y.; Wen, Y.; Li, S.; Du, S.; He, X.; Cai, L.; Li, Y.; Yang, L.; Gao, H.; Song, Y. *J. Am. Chem. Soc.* **2007**, *129*, 11674–11675.
(6) *Organic Electronics: Materials, Processing, Devices and Applications*; So, F., Ed.; CRC PressL Boca Raton, FL, 2010.
(7) *Principles of Nano-Optics*; Novotny, L.; Hecht, B., Eds.; Cambridge University Press: Cambridge, U.K., 2006.
(8) (a) Zhou, Y.; Liu, W.−J.; Ma, Y.; Wang, H.; Qi, L.; Cao, Y.; Wang, J.; Pei, J. *J. Am. Chem. Soc.* **2007**, *129*, 12386–12387. (b) Briseno, A. L.; Mannsfeld, S. C. B.; Lu, X.; Xiong, Y.; Jenekhe, S. A.; Bao, Z.; Xia, Y. *Nano Lett.* **2007**, *7*, 668–675.
(9) (a) Naddo, T; Che, Y.; Zhang, W.; Balakrishnan, K.; Yang, X.; Yen, M.; Zhao, J.; Moore, J. S.; Zang, L. *J. Am. Chem. Soc.* **2007**, *129*, 6978–6979. (b) Chen, Y.; Yang, X.; Loser, S.; Zang, L. *Nano Lett.* **2008**, *8*, 2219–2223.
(10) (a) Takazawa, K.; Kitahama, Y.; Kimura, Y.; Kido, G. *Nano Lett.* **2005**, *5*, 1293–1296. (b) Takazawa, K. *J. Phys. Chem. C* **2007**, *111*, 8671–8676. (c) Lebedenko, A. N.; Guralchuk, G. Y.; Sorokin, A. V.; Yefimova, S. L.; Malyukin, Y. V. *J. Phys. Chem. B* **2006**, *110*, 17772–17775. (d) Zhao, Y. S.; Xu, J.; Peng, A.; Fu, H.; Ma, Y.; Jiang, L.; Yao, J. *Angew. Chem., Int. Ed.* **2008**, *47*, 7301–7305. (f) Zhao, Y. S.; Peng, A.; Fu, H.; Ma, Y.; Yao, J. *Adv. Mater.* **2008**, *20*, 1661–1665. (g) Liao, Q.; Fu, H.; Yao, J. *Adv. Mater.* **2009**, *21*, 4153–4157. (h) Che, Y.; Yang, X.; Balakrishnan, K.; Zuo, J.; Zang, L. *Chem. Mater.* **2009**, *21*, 2930–2934.

Published on Web 05/21/2010

Chart 1. Molecular Structures of 1−5

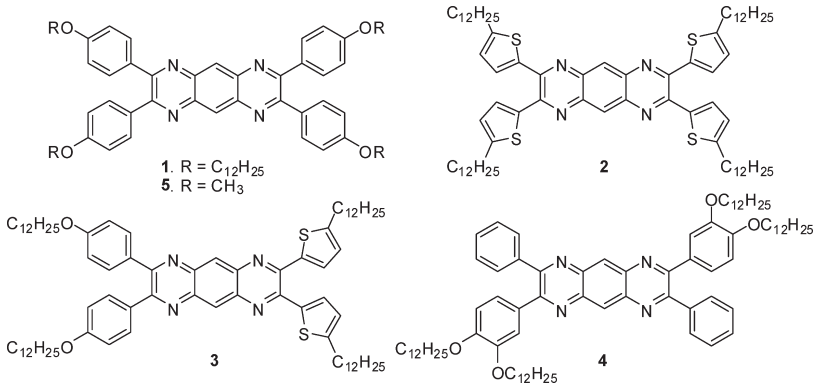

favor high fluorescence quantum yield in solid state.[11] On the other hand, highly fluorescent J-aggregates[12] are seldom observed, mainly because of their relatively small stokes shift, which leads to significant self-absorption lost during light propagation.[10] Though the H-aggregates of dyes have been reported as active waveguide fibers,[10a] how to weaken the unfavorably intermolecular $\pi-\pi$ interactions within stacks is worth exploring to further improve the waveguide performance of molecular assemblies.

To enhance fluorescent emission in solid state, we consider enlarging the intermolecular distance of adjacent aromatic rings by introducing steric hindrance; hence a nonplanar conjugated core was adopted to minimize the unfavorable intermolecular fluorescent quenching.[13] With this intention, a series of molecules based on tetrasubstituted pyrazino[2,3-g]quinoxaline (**PyQ**) units were developed, and the torsion of the adjacently attached aromatic rings embodied the desired steric hindrance. With its electron affinity and ease in syntheses, the **PyQ** unit is widely used in electroluminescent polymer materials,[14a,b] coupling of large aromatic cores (porphyrin[14c] and hexabenzocoronene[14d] as representatives) and optical electronic sensors of inorganic anions.[14e] Previous experiences also suggest that it is an effective way to engineer molecular aggregates by changing side groups.[6a,10h,15] Therefore, to promote the self-assembling process, we also introduced long alkyl chains as the structural group.

In this contribution, molecules **1**−**4** are designed with the same electron-deficient pyrazino[2,3-g]quinoxaline ring in the center and different electron-rich aromatic rings as periphery adjusting site for color and hindrance. Their structures are illustrated in Chart 1. **PyQ** is a highly symmetric core (D_{2h}), and both the molecules with maintained symmetry (**1** and **2**) and those with lowered symmetry introduced by periphery substitutes (**3** and **4**) were explored to demonstrate the favorable direction for the chemical modification of **PyQ** moiety. Though molecular assemblies are a combined result of molecular structure and growth conditions, understanding structure−property relationships of organic conjugated molecule is a prerequisite for controllable self-assembling process and is crucial to rational materials design. In addition, in solid state, the interactions between organic molecules are relatively weak compared with ionic bond and covalent bond, and the packing of molecular crystals is therefore generally complex yet molecular-shape-determined to some extent.[16] Hence, investigation on the geometric aspects of organic molecules are also worthwhile for functionalizing molecular assemblies. The effects of the molecular geometry and symmetry on their optical properties, crystal dimensions, liquid crystals (LC), and active waveguide properties are investigated in detail in the Results and Discussion section. The molecular structures and their photophyscial properties are correlated by computational methods on a single molecular level. Morphology and crystallography studies are then presented to build structure−property relationship in solid state. Liquid crystal behaviors are also discussed to provide deeper understanding of intermolecular interactions of molecules **1**−**4**. Finally, the waveguide behaviors of fibers of **1** and **2** are characterized to demonstrate the potential use of our materials as active waveguide fibers.

Results and Discussion

Synthesis. Scheme 1 illustrates the synthetic approaches to compounds **1**-**4**. This set of molecules were synthesized by the condensation of bezene-1,2,4,5-tetraamine and

(11) Jenekhe, S. A.; Osaheni, J. A. *Science* **1994**, *265*, 765.
(12) (a) *J-Aggregates*; Kobayashi, T, Ed.; World Science: Singapore, 1996. (b) Kaiser, T. E.; Stepanenko, V.; Würthner, F. *J. Am. Chem. Soc.* **2009**, *131*, 6719–6732.
(13) de Halleux, V.; Calbert, J.-P.; Brocorens, P.; Cornil, J.; Declercq, J.-P.; Brédas, J.-L.; Geerts, Y. *Adv. Funct. Mater.* **2004**, *14*, 649–659.
(14) (a) Cui, Y.; Zhang, X.; Jenekhe, S. A. *Macromolecules* **1999**, *32*, 3824–2826. (b) Zhu, Y.; Yen, C. T.; Jenekhe, S. A.; Chen, W. C. *Macromol. Rapid Commun.* **2004**, *25*, 1829–1834. (c) Crossley, M. J.; Thordarson, P. *Angew. Chem., Int. Ed.* **2002**, *41*, 1709–1013. (d) Fogel, Y.; Kastler, M.; Wang, Z.; Andrienko, D.; Bodwell, G. J.; Müllen, K. *J. Am. Chem. Soc.* **2007**, *129*, 11743–11749. (e) Anzenbacher, P.; Palacios, M. A.; Jursíková, K.; Marquez, M. *Org. Lett.* **2005**, *7*, 5027–5030.
(15) (a) Zang, L.; Che, Y.; Moore, J. S. *Acc. Chem. Res.* **2008**, *41*, 1596–1608. (b) Wang, J.; Yan, J.; Li, Z.; Han, J.; Ma, Y.; Bian, J.; Pei, J. *Chem.—Eur. J.* **2008**, *14*, 7760–7764. (c) Dautel, O. J.; Guillaume, W.; Almairac, R.; Flot, D.; Hirsch, L.; Lere-Porte, J.; Parneix, J.; Serein-Spirau, F.; Vignau, L.; Moreau, J. J. E. *J. Am. Chem. Soc.* **2006**, *128*, 4892–4901.
(16) Evans, R. C.; *An Introduction to Crystal Chemistry*, 2nd ed.; Cambridge University Press: Cambridge, U.K., 1964; Chapter 14, pp 352−356.

Scheme 1. Synthesis Routes of Compounds 1−4

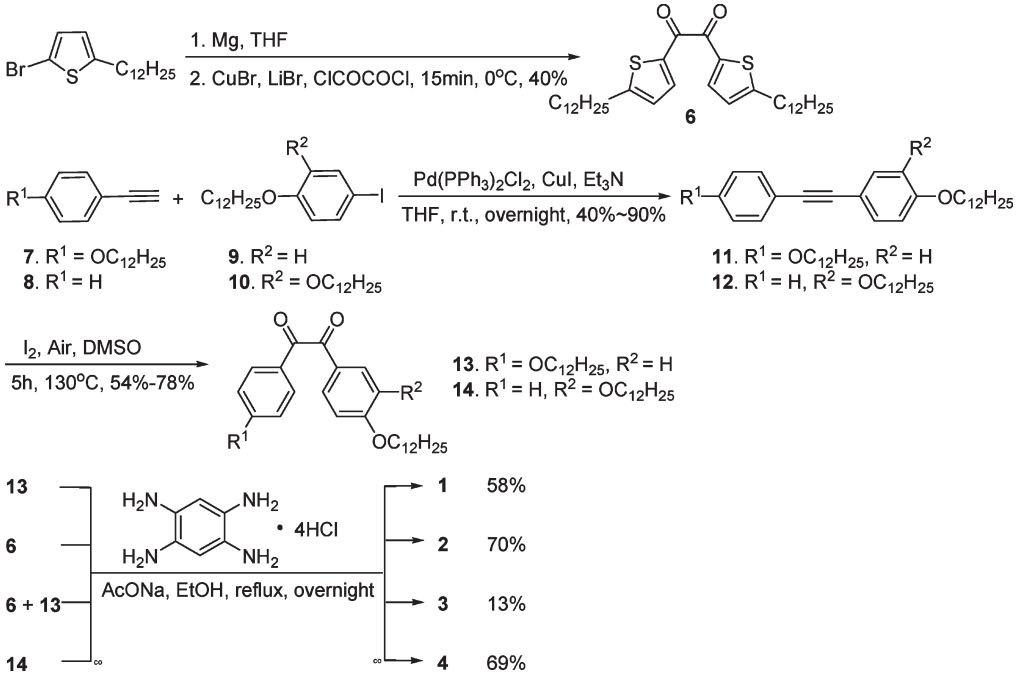

1,2-diketones. 2-Bromo-5-dodecylthiophene reacted with metal magnesium to convert to a Grignard reagent, followed by coupling with oxalyl chloride and lithium diarylcuprate to afford **6** in 40% yield. The oxidation of diarylethyne, which was prepared through a Sonogashira reaction between 1-ethynylbenzenes (**7** or **8**) and 1-iodobenzenes (**9** or **10**), gave compounds **11** or **12** in moderate yields. Finally, the condensation of bezene-1,2,4,5-tetraamine and 1,2-diketones (**6**, **13**, or **14**) afforded **1**, **2**, and **4**, respectively. Differing from the literature reports on *o*-quinone,[17] the yield of cross-condensation product **3** was quite low (13%) no matter which diketone (**6** or **13**) was added first. This may result from a lowered intramolecular ring-closing rate caused by steric hindrance of two adjacent aromatic rings. Another notable result is that only anti product was obtained in the synthesis of **4**, which also indicated a long period of dynamic-chemical-bonding process before intramolecular ring closure. Thus, in this series, the molecules with symmetric center are more favorable as organic materials from the standpoint of the ease of synthesis. The new compounds were readily soluble in common organic solvents, such as toluene, THF, DMSO, and CH_2Cl_2. The structures and purity of all new compounds were fully characterized and verified by ^1H and ^{13}C NMR, elemental analysis, and HRMS.

Photophysical Properties. The absorption and photoluminescence (PL) spectra of molecules **1**−**4** were measured in dilute CH_2Cl_2 solution as presented in Figure 1. Table 1 summarizes all photophysical properties of molecules **1**−**4** in dilute solution. Molecules **1**, **2**, and **3** exhibited the similar absorption features with two absorption bands. For molecule **1**, the absorption maxima peak at

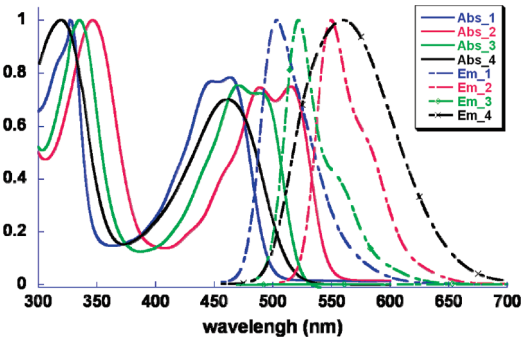

Figure 1. Absorption (solid line) and PL (dashed line) spectra of molecule **1**−**4** in dichloromethane solution (1×10^{-5} M). All PL spectra were collected under excitation at the maximum absorption peak of the correspond compounds.

about 464 nm, 449 nm, and 327 nm. However, in comparison with molecule **1**, for **2**, all the three peaks red-shift 20−50 nm, indicating that the effective conjugation length is increased after introducing the thiophene units in place of the phenyl rings in **1**. This may attributed to that the adjacent five-member rings have smaller steric hindrance than the six member rings and thus the whole molecule of **2** is better coplanar. It is also observed that the three wavelengths of the absorption maximum (λ_{max}) for **3** are between those of **1** and **2**. Also, for **1**, **2**, and **3**, their absorption and PL features are quite similar in terms of vibration structures (absorption peak in 400−500 nm and emission peak in 500−550 nm), full width at half-maximum (fwhm, 34−49 nm) and Stokes shifts (28−38 nm). Molecule **4** shows the absorption features very similar to **1**. The investigation of the absorption features of molecules **1**−**4** indicate the conjugated nature of molecule **1**−**4**, though the steric hindrance between adjacent periphery rings has undermined the coplanarity of the whole molecule. As shown in Figure S1 in the Supporting Information, computational

(17) Sendt, K.; Johnston, L. A.; Hough, W. A.; Crossley, M. J.; Hush, N. S.; Reimers, J. R. *J. Am. Chem. Soc.* **2002**, *124*, 9299–9309.

Table 1. Summary of optical properties, crystal dimensions, and thermo Transitions of 1−4

	optical properties					
	1×10^{-5} M in DCM					
molecules	λ_{abs} (nm) (lgε) (dm^3 mol^{-1} cm^{-1})	λ_{PL} (fwhm) (nm)	Stokes shift (nm)	transition dipole moment (μ_e) (D)	microfiber dimensions	thermo transition (°C) and *d*-spacings (Å)[a]
1	464 (4.98), 449 (4.98), 327 (5.08)	502 (47)	39	13	length, 100−1000 μm; width, 1−5 μm	heating, Cr (27.4)−103-Sm (35.8)−172−I; cooling: I −166−Sm (34.8)−73−Cr_1 (34.7)−42−Cr_2 (34.0)−18−Cr_3
2	515 (4.26), 489 (4.26), 346 (4.36)	543 (49)	28	5	length, 100−1000 μm; width, 0.5−3 μm	heating, Cr−97−I; cooling, I−57−Cr
3	488 (4.76), 471 (4.78), 335 (4.90)	522 (34)	34		length, 5−10 μm; width, 1−2 μm	heating, Cr−81−I; cooling, I−76−Cr
4	450 (4.46), 309 (4.61)	560 (93)	110	25	length, > 100 μm; width, 100 nm	heating: Cr (36.7)−48−Sm (39.6)−78−N−114−I; cooling, I−102−N−55−Sm (40.0)−37−Cr (36.7)

[a] Cr stands for crystal; Sm stands for smectic phase, detailed discussion see the text; N stands for nematic phase; I stands for isotropic liquid.

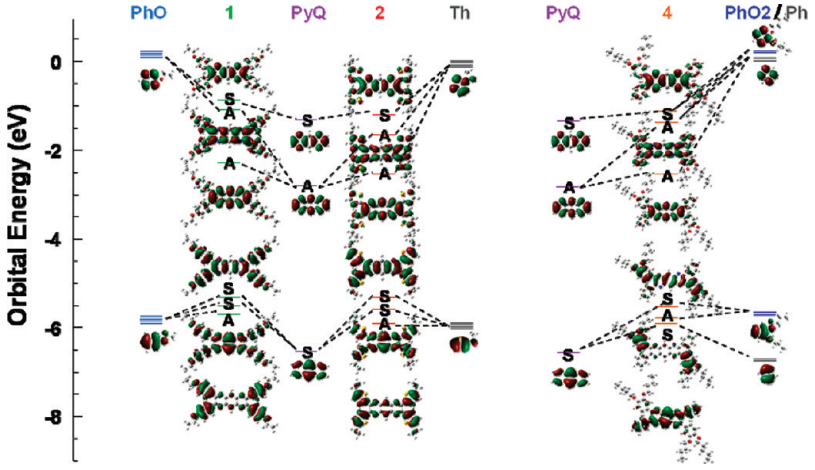

Figure 2. Graphical representation of calculated molecular orbitals of molecule **1**, **2**, **4** and the core **PyQ**. The long alkyl chains were shortened to ethyl or butyl for brevity. A represents that the corresponding orbital is antisymmetrical to symceter; S represents symmetrical to symceter; Dashed lines indicate correlations between the MOs of **1**, **2**, and **4**, those of periphery electron rich rings and **PyQ** according to orbital symmetry and the numbers of nodes. **PhO** stands for ethoxylbenzene, **Th** for 2-ethylthiophene, **Ph** for benzene, **PhO2** for 1,2-dibutoxylbenzene, respectively.

results, which were consistent with the experimental absorption spectra, further confirmed the electronic communication between periphery rings and the core by visualizing highly delocalized HOMOs. Figure 2 shows simulated molecular orbital (MO) diagram of molecules **1**, **2**, and **4**, in which **2** had more delocalized MOs than **1**.

On the basis of their conjugated nature, the donor and acceptor interactions of **1**−**4** could be qualitatively analyzed. In a grossly simplified consideration, MOs of molecules **1**−**4** were regarded as a result of linear combination of MOs of **PyQ** and those of periphery aromatic rings.[18] As shown in Figure 2 and Table S1 in the Supporting Information, the separately calculated results of the MOs of the core and the periphery substitutes indicate that the HOMOs of electron-rich substitutes are about 0.8 eV higher than that of **PyQ**, whose LUMO is around 3 eV lower than those of electron rich rings. Then, the previous MOs of each segment are identified from new synthesized molecules by symmetry and the numbers of nodes.[19] For example, the previous HOMO of **PyQ** is symmetrical to symceter (a *g* orbital, labeled by S) with three nodes, and the two occupied MOs in newly synthesized molecules with the same *g* symmetry and three nodes in the core are therefore correlated with the HOMO of **PyQ**. The qualitatively correlating diagram (as illustrated in Figure 2) shows that the HOMOs of periphery rings have contributed most of HOMO, HOMO-1, and HOMO-2 because of the energy level proximity and quantitative abundance, whereas the core has made up most of the new LUMO because of its much lower LUMO energy level. Considering that the HOMO is a potential electron donor, whereas the LUMO is a potential electron acceptor, this set of molecules **1**−**4** could also be classified as D−A systems.

In addition to the common photophysical features of molecules **1**−**4**, comparing the different donor segments is helpful to future rational design of optical material. A notable phenomenon is that the extinction coefficient of **1** ($lg\varepsilon = 4.98$) is five times large as that of **2** ($lg\varepsilon = 4.26$) (see Table 1). This difference could partly be attributable to

(18) Combs, L. L. *Int. J. Quantum Chem.* **1977**, *11*, 1001–1004.
(19) (a) Lin, H.-C.; Jin, B.-Y. *J. Phys. Chem. A* **2008**, *112*, 2948–2954. (b) Lois, S.; Florès, J.-C.; Lère-Porte, J.-P.; Serein-Spirau, F.; Moreau, J. J. E.; Miqueu, K.; Sotiropoulos, J.-M.; Baylère, P.; Tillard, M.; Belin, C. *Eur. J. Org. Chem.* **2007**, 4019–4031.

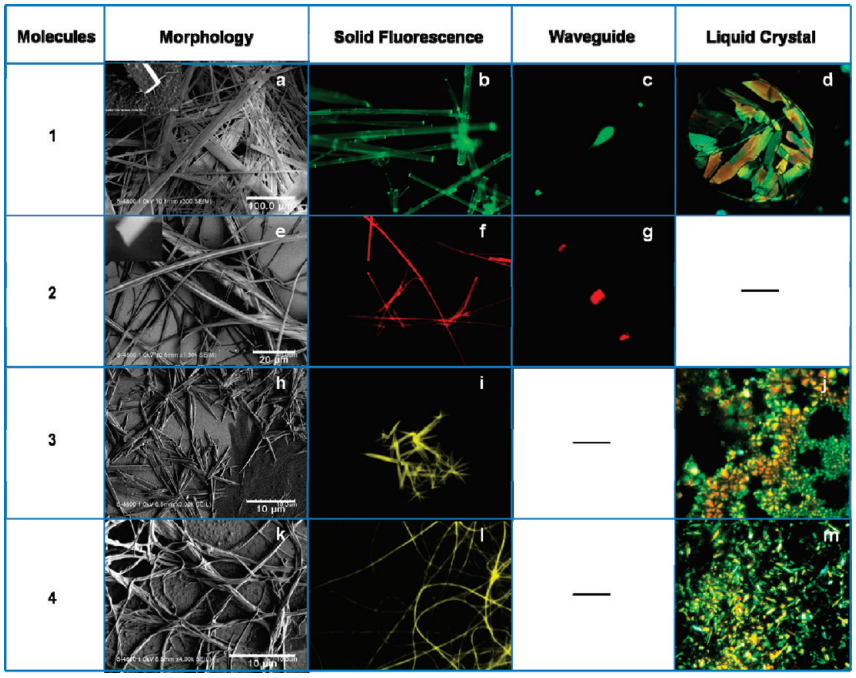

Figure 3. (a, e, h, k) SEM images of the morphologies of **1**−**4**, respectively (insets of a and e present flat and smooth end surfaces); (b, f, i, l) fluorescent microscope photographs of the morphologies **1**−**4** that were grown under the conditions same as that of the SEM images; (c, g) fluorescent microscope photographs of the wires of **1** and **2**, respectively, taken under spot laser lighting, displaying the optical waveguide property; (d, j, m) polarized optical microscope (POM) photographs of **1** (88 °C, cooling), **3** (84 °C, heating), and **4** (125 °C, heating), respectively.

the greater transition dipole moment of **1** (13 D) than that of **2** (5 D), because the absorption strength (oscillator strength f) is in direct proportion to the square of transition dipole moment (μ_e).[20] However, **4** could not be compared in the same way for its molecular symmetry different from **1** and **2**. To enable calculation by Lippert−Mataga equation,[21] we had technically made an assumption that the flexible alkyl chains were negligible to the effective cavity radius of these molecules (see Figure S3 in the Supporting Information). Compound **5** (Chart 1) was synthesized as a model to test this assumption. The result that the difference of the μ_e values of **1** (13 D) and **5** (14 D) is insignificant, leading to the validity of this simplified method. Another notable phenomenon is that **4** losses its vibration structure in both absorption and emission spectra in comparison with **1**−**3**, and has a much broadened emission peak with a large Stokes shift. The disappearance of vibration structure of **4** could be ascribed to the reduction of its molecular symmetry, because the molecular vibrations are coupled with electron transitions. However, the broadening of emission spectra of **4** could not simply explained by the vibration pattern. Actually, the HOMO-1 and LUMO of **4** are both u MOs (antisymmetrical to symcenter, labeled by A), while according to Laporte selective rule the transition u MO and u MO is forbidden.[22] Hence, there is no radiative relaxation pathway from LUMO to HOMO-1. Also taking its large μ_e (25 D) into consideration, an internal charge transfer (ICT) state is suggested to exist in **4**′s excited state,[23] which becomes dominant as solvent polarity increases.

Morphology and Structural Analysis. As discussed in the previous session, the molecular symmetry plays an important role in single molecular optical behaviors: the absence of mirror planes (**4** compared with **1** and **2**) is more influential to the shape of molecular optical spectra than the absence of symmetrical center (**3**). At the level of molecular aggregate or crystal, the effect of molecular symmetry is more pronounced. As shown in Figure 3 and Table 1, all micronano structures of **1**−**4** grown from solution are fibrous. It is very interesting that the absence of symmetrical center leads to shortened fiber length (10 μm in Figure 3h compared with >100 μm in panels a and e in Figure 3); while the absence of mirror planes leads to narrowed fiber width (100 nm in Figure 3k compared with 1−5 μm in Figures 3a and 3e). To relate the molecular structure to the macroscopic morphology, we obtained the single-crystal structure of **1**. Figure 4 shows that packing of alkyl chains is more crucial in determining crystal structure than the stacking of π planes because of the following observations: (1) all alkyl chains are completely parallel and overlapped, which maximized the interactions between alkyl chains; (2) no typical distance of $\pi-\pi$ stacking (3.4 Å) is found in the single-crystal structure. Hence, the reason that molecular symmetry affects macroscopic morphology is highly related to the difference of arrangement of alkyl chains.

To further illustrate the molecular packing in the nanofibers of **1**, two-dimensional wide-angle X-ray diffraction (2D-WAXD) experiments were conducted. 2D-WAXD

(20) Zollinger, H.; *Color Chemistry: Syntheses, Properties and Applications of Organic Dyes and Pigments*, rev. ed.; Wiley-VCH: Zürich, Switzerland, 2003; Chapter 2, pp 31−32.
(21) Lakowicz, J. R.; *Principles of Fluorescence Spectroscopy*, Springer Science and Business Media, 2006, New York, p 208.
(22) Laporte, O.; Meggers, W. F. *J. Opt. Soc. Am.* **1925**, *11*, 459–460.
(23) Singh, M. K.; Pal, H.; Bhasikuttan, A. C.; Spare, A. V. *Photochem. Photobiol.* **1998**, *68*, 32–38.

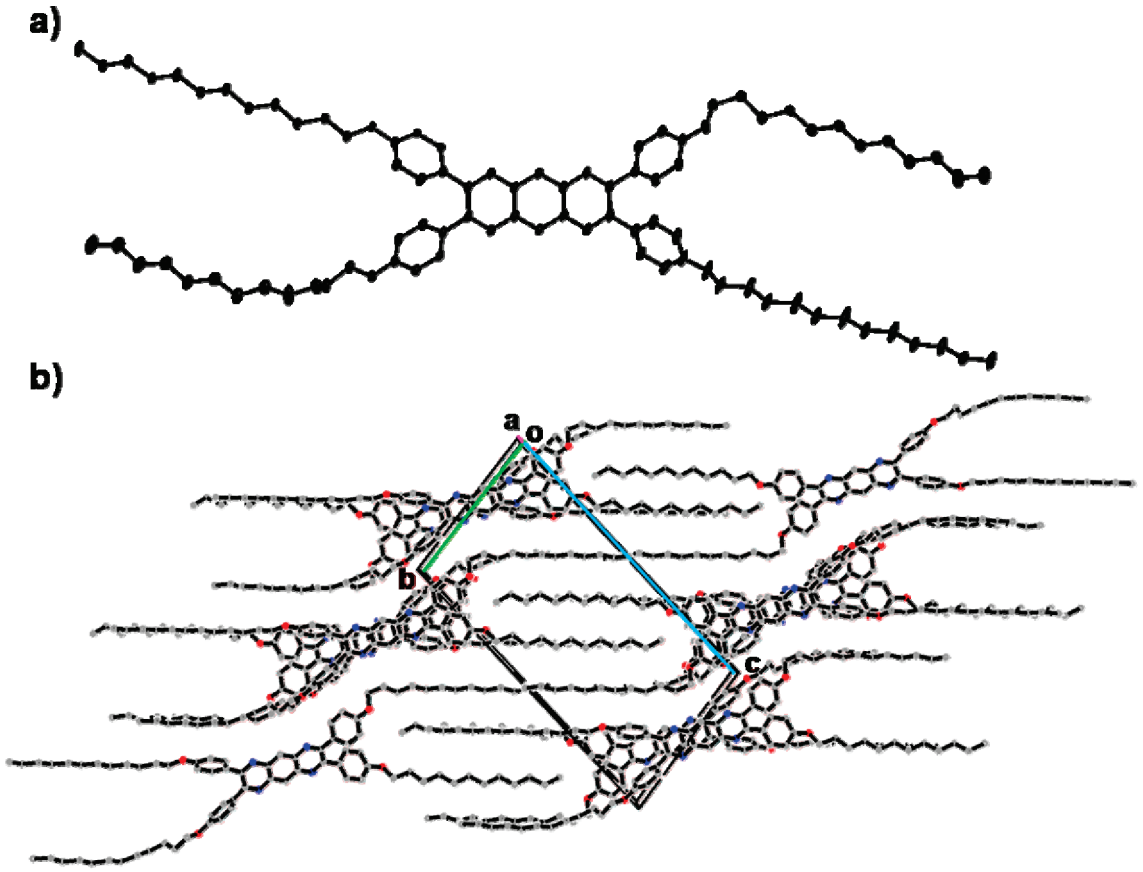

Figure 4. Single-crystal structure of **1**: (a) geometry of a single molecule in the crystal, in which the two alkyl chains in diagonal are all-trans conformation, whereas the other two adopt the same direction with all-trans chains by one gauche turn; (b) single-crystal structure of **1**, $a = 9.21$ Å, $b = 14.6$ Å, $c = 27.96$ Å, $\alpha = 79.02°$, $\beta = 84.70°$, $\gamma = 80.96°$; the shading circle represents an aromatic column; the aromatic columns and the alkyl chains form a layered structure.

technique has been widely used in the structure elucidations of the crystal or liquid crystal phase of polymers[24a,b] and small organic molecules.[24c] To prepare appropriate sample for 2D-WAXD (Figure 5a), a solvent-evaporation-assisted dipping method for the growth of nanowire arrays was adopted.[25] Molecule **1** was first dissolved in a solvent mixture of chloroform and ethanol. Because chloroform is more volatile than ethanol and the total volume of the solution of **1** was decreasing with time, the nanowires of **1** precipitated and arrayed on the surface of aluminum foil which was partially immersed in the solution.[25b] Figure 5c of a SEM image shows that the arrays of nanowires, though not perfect, do align parallel with each other in certain domains. The 2D-WAXD patterns were obtained under both vertical and parallel geometries (Figure 5d,f) and the corresponding integral XRD spectra were indexed by using the cell parameters of the single crystal of **1** (Figure 5e,g). The peaks from 18 to 25° in Figure 5e are much stronger than that of Figure 5g, which indicates that the normal directions of the lattice planes corresponding to 18−25° are in parallel, at least almost in parallel, with the direction of nanofibers. The spots in 2D-WAXD pattern obtained from vertical geometry are correlated with the diffraction of certain lattice planes of the crystal of **1** (Figure 6, also see Figure S5 and Table S2 in the Supporting Information).[26] The (001) diffraction appears on the equator, corresponding to a *d*-spacing of 27.4 Å, which represents the distance between two adjacent columns of π planes across the alkyl chain layer. The (210) plane is near vertical to the plane (001), of which a *d*-spacing of 4.5 Å is the distance of the adjacent π planes within the column. The planes of (223), ($2\overline{1}3$) and are parallel to the direction of alkyl chains, and thus the *d*-spacings of 4.0 and 3.8 Å stand for the distances of the adjacent alkyl chains within the alkyl chain layer. It is notable that the distances of lattice planes related to the alkyl tails of **1** (4.0 and 3.8 Å) are almost the same as that of polyethylene chain packed in orthorhombic crystal lattice,[27] which further suggests that the driving force of

(24) (a) Kasai, N.; Kakudo, M. *X-Ray Diffraction by Macromolecules*; Springer Series in Chemical Physics; Springer, Heideburge, 2005; Vol. *80*. (b) Yin, X.; Ye, C.; Ma, X.; Chen, E.; Qi, X.; Duan, X.; Wan, X.; Cheng, S. Z. D.; Zhou, Q. *J. Am. Chem. Soc.* **2003**, *125*, 6854–6855. (c) Fischbach, I.; Pakula, T.; Minkin, P.; Fechtenkötter, A.; Müllen, K.; Spiess, H. W. *J. Phys. Chem. B* **2002**, *106*, 6408–6418.

(25) (a) Kaslter, M.; Pisula, W.; Wasserfallen, D.; Pakula, T.; Müllen, K. *J. Am. Chem. Soc.* **2005**, *127*, 4286–4296. (b) Zhang, C.; Zhang, X.; Zhang, X.; Fan, X.; Jie, J.; Chang, J. C.; Lee, C.-S.; Zhang, W.; Lee, S.-T. *Adv. Mater.* **2008**, *20*, 1716–1720.

(26) Both the distance and angle and of certain lattice plane were calculated and compared in this identification process to ensure correctness of matching. It is worth noting that the diffraction speckles in high θ region (with the lattice distance of 3−5 Å) are actually corresponding to several lattice planes instead of a single one, thus the lattice index from 15 to 25° in panels e and g in Figure 5 and lattice planes displayed in Figure 6 (except 001) are only representatives of all lattice planes that contribute to certain diffraction speckle. For detailed calculations and comparisons, see Table S2 in the Supporting Information.

(27) Yin, Li.; Chen, J.; Yang, X.; Zhou, E. *Polymer* **2003**, *44*, 6489–6493.

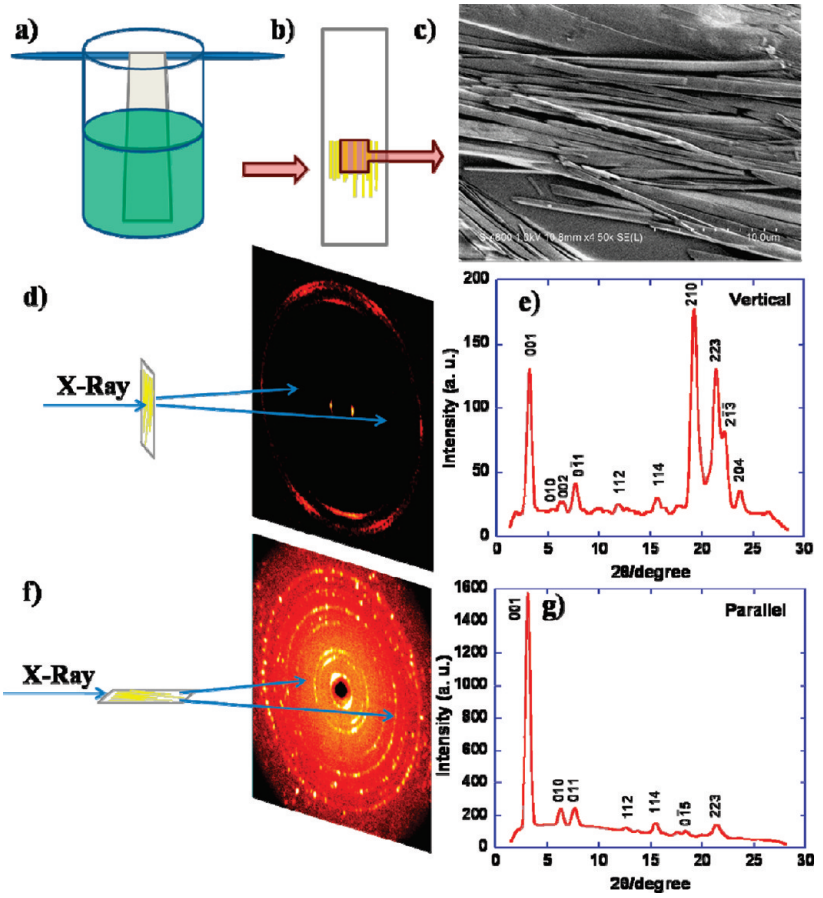

Figure 5. (a,b) Preparation method for 2D-WAXD sample. A solution of **1** in chloroform/ethanol = 1/4 (V/V) (5 mg/mL) in a 10 mL bottle was set in air for 2 days. When the good solvent of chloroform was evaporated, the nanofibers of **1** were deposited on the surface of a aluminum foil with the fiber axis preferentially perpendicular to the solution surface. (c) SEM images of nanowire arrays on the aluminum foil. (d, f): diffraction geometris of 2D-XRD experiments (2θ of 1.2−28.0°, recorded, step 0.02°) with X-ray incident beam vertical to and parallel to the nanowires, respectively. (e, g) Integral 2D-WAXD patterns of d and f, respectively; the peaks are indexed on the basis of the single-crystal cell parameters of **1**.

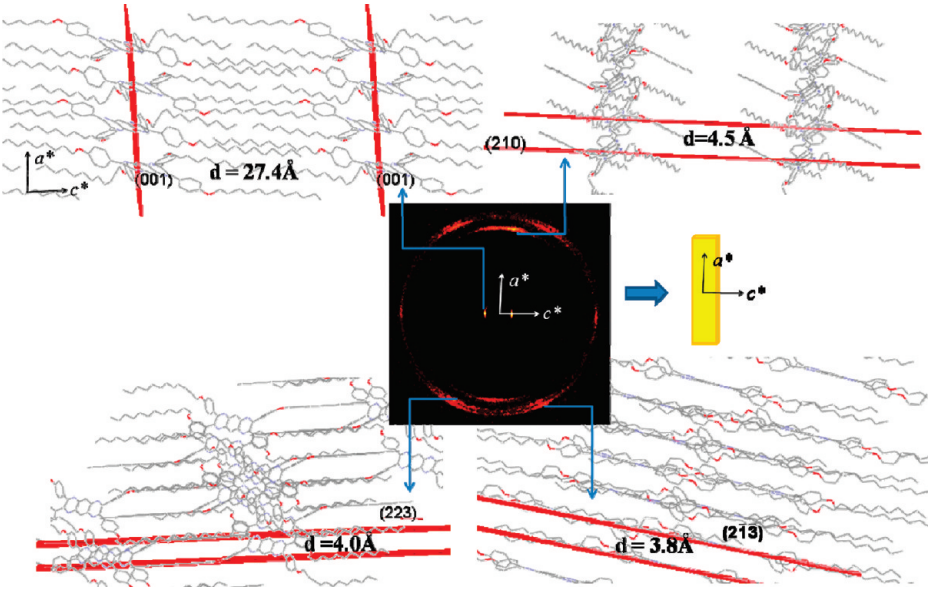

Figure 6. Indexing 2D-WAXD patterns on the basis of the single crystal structure of **1**; the yellow ribbon represents a microfiber of **1** with the a^* axis parallel to the long axis of the fiber.

the packing of **1** in crystal state is largely related to the interaction among the alkyl chains. As mentioned above, the (001) diffraction is located on the equator, indicating that the c^* is perpendicular to the nanofiber axis which is along the meridian. Hence, the end facet of nanofibers of **1** should be almost parallel to the π plane of **1**. This

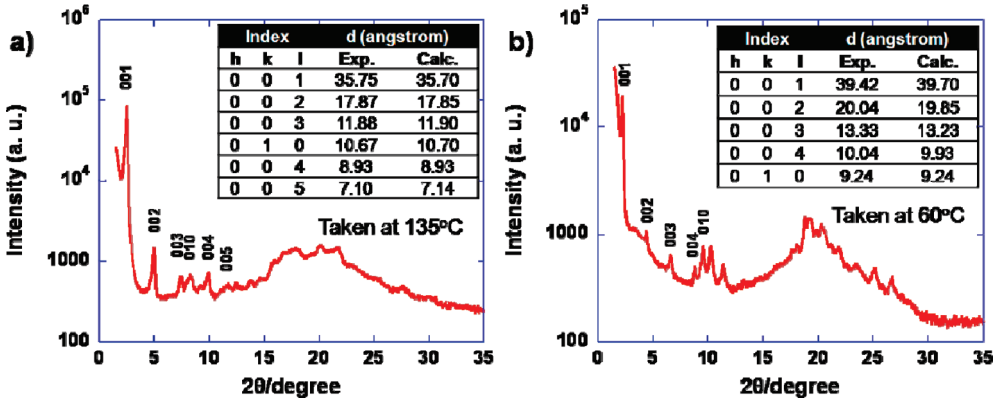

Figure 7. (a, b) WAXD profiles of **1** at 135 °C and **4** at 60 °C, respectively. The intersections are the corresponding indexes.

conclusion is also in agreement with the structure analysis based on 2D-WAXD patterns given by Müllen et al.[24c,25a]

Because the molecular weights (1185−1126 D) and the mass percents of alkyl chains (57−60%) of **1**−**4** are almost the same, the conclusion drawn from the crystal structure of **1** should be applicable to the structures of −-**4** to some extent. However, we note that the angles of five-member rings with respect to the **PyQ** core in **3**,are different from those of six-member rings in **1**. As a result, it is unfavorable for **3** to achieve all-parallel conformation for alkyl chains. Though alkyl chains are flexible in some way, minor angle deviation may lead to systematically deformation resulting in a fusiform morphology. For **4**, because of the nearer position of two adjacent alkyl chains, they would pack with each other in the solid state, and thus one pair of intermolecular interaction is replaced by one pair of intramolecular interaction in comparison with **1**. One result of this change is that intermolecular packing between two adjacent molecules along molecular long axis (they clipped with each other in **1**) would be weakened, which may be a reasonable explanation for the narrowed fiber width of **4**. Another result is that melt point of **4** (114 °C) is much lower than that of **1** (172 °C, Table 1).

Liquid Crystals. The formation of mesophases of **1** and **4** were also observed.[28] **1** displayed a typical mosaic texture of smectic (Sm) phase[29] at above 103 °C (Figure 3d). Combining the WAXD result recorded at 135 °C (Figure 7a), we consider that the LC phase of **1** has a layered structure. Molecule **3** did not have a stable liquid crystal phase region, but its focal conic texture, which is typical in SmA phases,[29a] was observed when the sample was prepared by drop cast. For **4**, identifiable texture of LC phase was not observed; but WAXD result shows that it actually has a layered structure at elevated temperatures (Figure 7b). For both **1** and **4**, it is worth noting that a diffraction which can be assigned to (010) diffraction appear in the low-angle region (Figure 7a,b), suggesting that **1** and **4** have a higher position order than the molecules forming simple SmA or SmC with a 1D positional order.[30] The *d*-spacing of the (010) plane of ∼10 Å is fairly equal to the width of the molecules, whereas the *d*-spacing of the (001) is close to the molecular length calculated with an assumption that the alkyl tails are in an all-trans conformation. However, although the layered structures render the (00*l*) diffractions with *l* up to 5 for **1** and for **4**, only (010) diffractions are observed for these two molecules. Therefore, **1** and **4** do not possess a perfect 2D positional order that can be detected in a typical columnar LC phase. Two factors are considered responsible to the formation of these apparently transition LC states that have the order higher than Sm phase but lower than columnar phase. First, the orthogonal interactions of alkyl chains and π planes make the cores and coronas tend to segregate, thus a layered structure has formed like some surfactants with along alkyl chains.[31] Second, the lubrication provided by flexible chains are important for discotic mesogens to form column phase;[30] however, the large aspect ratio (5:1)[32] of molecule **1** and molecule **4** leads to an extremely anisotropic distribution of alky chains and results in a 2D continuous layer of aromatic cores (based on single-crystal structure of **1**, Figure 4). As a result, the fact that the aromatic core columns were not well-separated by flexible alkyl chains has weakened the columnar feature, though position order exists to some extent within each layer. It is also notable that the *d*-spacing (Table 1) of the layered structure of **4** (39.4−40.0 Å) is larger than that of **1** (34.8−35.8 Å). As the lengths of **1** and **4** along molecular long axis are the same, this observation further supports the weakened attachments between layers of **4** in comparison with **1**. Moreover, because the shape of **4** is rather calamitic (rod-like) than sanidic (lath-like, and the shape of **1**−**3** are more sanidic), **4** also has a nematic phase at above 78 °C (Table 1). Here, though the phase identification is preliminary, we can still conclude that the different LC behaviors of **1** and **4** are largely dependent on the

(28) The absence of stable mesophase of molecules containing thiophene segments (**2** and **3**) is probably due to the lack of polar groups between the aromatic core and these alkyl chains, see: Tschierske, C. *J. Mater. Chem.* **1998**, *8*, 1485–1508.

(29) (a) Dierking, I.; *Textures of Liquid Crystals*; Wiley-VCH: Weinheim, Germany, 2003; p 136. (b) Liu, P.; Wu, Y.; Pan, H.; Li, Y.; Gardner, S.; Ong, B. S.; Zhu, S. *Chem. Mater.* **2009**, *13*, 2727–2732.

(30) De Genes, P.-G.; Prost, J. *The Physcis of Liquid Crystals*; Oxford University Press: Oxford, U.K., 1995; pp 2−6.

(31) Chae, P. S.; Guzel, I. A.; Gellman, S. H. *J. Am. Chem. Soc.* **2010**, *132*, 1953–1959.

(32) The aspect ratio is measured according to the single-crystal structure of 1; the ratio of the length of molecular long axis and that of molecular short axis is 4.8:1.

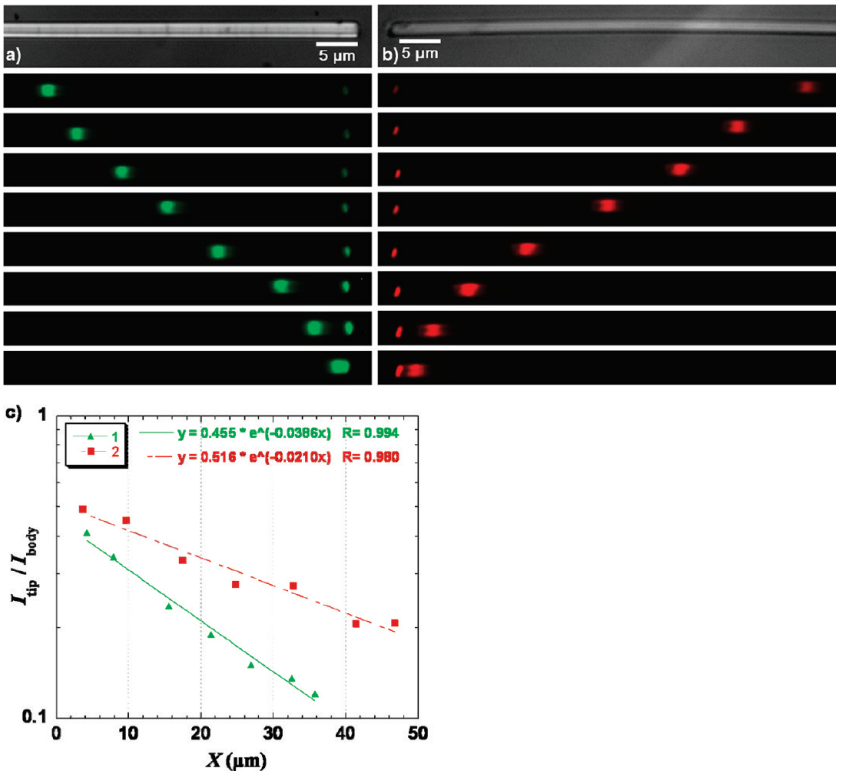

Figure 8. Waveguide characterizations of the microfibers of **1** and **2**. (a, b) Fluorescent microscope photographs of the microfibers of **1** and **2** (gray value images and painted with false color); (c) optical losses. The ratio of intensity I_{tip}/I_{body} against distance X between the excited spot and the emitting tips. The curves were fitted by an exponential decay function $I_{tip}/I_{body} = A\exp(-\alpha X)$, where A and α are fitting parameters and α represents the optical loss (dB/μm).

intermolecular forces and the molecular shape (aspect ratio).

Low-Loss Waveguide Fibers. Another notable phenomenon is that **1**−**4** have remained fairly high fluorescence in the solid state (Figure 3 and Figure S4 in the Supporting Information). Especially, the fibers of **1** and **2** with their high crystallinity (for **2**, see XRD and TEM results in Figure S8 in the Supporting Information) have active waveguide property (Figure 3c,g). **3** and **4** could not be applied as 1D waveguide materials, because that the nanostructure of **3** absent a distinct end face and the fiber width of **4** is quite limited.[10a] In this investigation, the intensity at body excited site (I_{body}) and emitting tip (I_{tip}) were recorded and the optical loss coefficient (α) was calculated by single exponential fitting [I_{body}/I_{tip} = Aexp(−αX), where X is the distance between the exciting site and emitting tip]. Because the total gray values were employed to analyze the optical loss, the obtained α is an average evaluation of the waveguide efficiency of **1** and **2** through their full fluorescent region. The I_{body} was adopted as reference to reduce the fluctuation of the overlap area of laser spot and fiber surface. The physical meaning of fitting parameter A is suggested to be the ratio of the amount of light escaping from the excitation spot and that of light propagating along the fiber.[33] The other fitting parameter α presents the optical loss for a guide length of 1 μm. The results of α are 0.024−0.039 dB/μm of **1** and 0.014−0.043 dB/μm of **2** (Figure 8) are comparable to those of low-loss inorganic nanowires (0.026 dB/μm)[34a−c] and are lower than those of previously reported organic waveguide materials, such as dye aggregates (0.5 dB/μm)[10b] and polyfluoroene (0.48 dB/μm).[34d] If the optical losses were caused by reabsorption, α should be proportional to extinction coefficient ε.[10b] Divided by the body concentration 2.2 mol/L of **1** (estimated from the cell volume of the single crystal of **1** as 3639 Å^3), the α of **1** could be converted to 180 L mol^{-1} cm^{-1}, which is equal to 0.2% of the ε of **1**′s absoption peak at 464 nm. Hence, the overlap of the absorption and fluorescent spectra of **1** is negligible. Despite the reduced reabsorption, there are other two important factors that may contribute to the excellent optical waveguide behaviors of **1** and **2**: (1) both the fibers of **1** and **2** have smooth surface and distinctly flat end

(33) The discussion on the physical meaning of A could not be found in previous literature to the best of our effort, though this fitting method was widely used, see ref 10. For one-dimensional waveguide, the propagating direction possesses one dimension of the three dimensions of space, hence theoretical value of A would be 1/2 (= (1/3)/(2/3)) if the fluorescent light at excitation spot is isotropic. According to our result, the experimental value of A is indeed around 0.5, and hence the physical meaning of A is reasonable.

(34) (a) Law, M.; Sirbuly, D. J.; Johnson, J. C.; Goldberger, J.; Saykally, R. J.; Yang, P. *Science* **2004**, *305*, 1269–1273. (b) Pan, A.; Liu, D.; Liu, R.; Wang, F.; Zhu, X.; Zou, B. *Small* **2005**, *1*, 980–983. (c) Barrelet, C. J.; Graytak, A. B.; Lieber, C. M. *Nano Lett.* **2004**, *4*, 1981–1985. (d) O' Carroll, D.; Lieberwirth, I.; Redmond, G. *Small* **2007**, *3*, 1178–1183.

(35) The emitting spectra of **1**−**4**, see Figure S4 in the Supporting Information: only slight shifts of the absorption and emission maxima of **1**, **3**, and **4** were observed in going from solution to solid; the emerging vibrational structure of the absorption spectra of **1**−**4** were explained by the restriction of rotation freedom of the periphery rings; the bathochromic shift of the fluorescent band of **2** is ascribed to the conformational change of thiophene rings in solid state.

facets which have minimized the optical losses caused by scattering; (2) the steric hindrance between nonplanar π planes minimizes effective $\pi-\pi$ interaction (4.5 Å), thus the optical features in single molecular level remains in the solid state.[35] Similar conclusion has been drawn by Geerts et al. in the study of the high fluorescent solids of tetraphenylpyrene derivatives.[13]

Conclusion

In summary, we have developed pyrazino[2,3-g]quinoxaline derivatives **1**−**4** for high efficiency active waveguide fibers. The effects of the molecular geometry and symmetry on their optical properties, crystal dimensions, and liquid crystal behaviors were investigated by a combined application of optical spectroscopy, microscopy, single crystal analysis, and 1D- and 2D-WAXD techniques. At a single molecular level, the geometrical difference of steric hindrance between 5-member aromatic ring and 6-member aromatic ring leads to different extent of conjugation. The calculated orbital diagram under the principle of linear combination of molecular orbitals reveals the D−A feature of this set of molecules. The effects of molecular symmetry of **1**−**4** not only are expressed in electron-vibration spectra, but also are crucial to the aggregates morphology. The absence of symmetrical center in molecule is more unfavorable to fibrous growth than the absence of mirror planes, because in this series the alkyl chains tend to array in parallel and their interactions are influential to the arrangements of such molecules with nonplanar aromatic core. The liquid crystal behaviors of **1** and **4** further confirm the role which the alkyl chains play in the molecular packing: (1) they provide the microsegregation force; (2) their positions strongly influence the molecular anisotropy and the strength of intermolecular interactions. The structure−property investigations have provided a deeper understanding for the structure and intermolecular interactions of such molecular aggregates. In addition, our analyses on molecular arrangements in the microfibers by combining single-crystal and 2D-WAXD techniques may be a general method for elucidating fiber-shape organic assembles.

The crystalline fibrous aggregates of **1** and **2** were then proved to be low-loss active waveguide fibers (0.02−0.05 dB/μm), which suggests the success of our strategy of integrating the nonplanar aromatic core to enlarge the distance of molecular stacks (4.5 Å) and the alkyl chain as structural group to promote self-assembly. Hence, this strategy may be a promising approach to achieve crystalline fluorescent materials for waveguides and lasers.

Experimental Section

General Methods. Commercial chemicals were purchased and used as received. ^{1}H and ^{13}C NMR spectra were recorded on Varian Mercury (200 MHz or 300 MHz) at room temperature in $CDCl_3$. All chemical shifts were reported in parts per million (ppm). MS spectra were recorded on Fourier Transform Ion Cyclotron Resonance Mass Spectrometer (Bruker APEX IV). The microfibers of **1**−**4** were obtained by vapor diffusion method: 1×10^{-4} M solutions of **1**−**4** in tolene and ethanol were placed in a sealed bottle at room temperature and the microfibers of **1**−**4** gradually precipitated during 1 week. Absorption spectra were recorded on PerkinElmer Lambda 35 UV−vis spectrometer. PL spectra were carried out on F4500 FL Spectrophotometer. Differential scanning calorimetry (DSC) analyses were performed on a METTER TOLEDO Instrument DSC822e calorimeter. Polarized microscopic (POM) pictures were recorded on DMLP Polar Microscope with Heat Stage produced by Leica. The SEM images were recorded on a S4800 cold field-emission scanning microscope. 1D WAXD was performed on a Philips X'pert Pro with an X'Celerator detector and 2D WAXD experiments were carried out on a Bruker D8 DISCOVER with a GADDS detector. The X-ray wavelength was 0.154 nm.

Computational Detail. Atomic structures of **1**, **2**, **4**, and other molecular segments were optimized with density functional theory (DFT) calculations using the B3LYP/6-31G (d). Molecular orbital shapes and energies discussed in the text are those calculated at the optimized geometries. Orbital pictures were plotted with Gaussview4.1. Electronic excitation energies and oscillation strengths were computed for the 60 lowest singlet excited electronic states of **1** and **2** with timedependent (TD) DFT calculations. In plotting computed electronic spectra, a Lorentzian line width of 0.15 eV was superimposed to each computed intensity. All quantum-chemical calculations were performed with the Gaussian03 package.

Waveguide Characterization. The laser was provided by Coherent CUBE-405−50C and introduced into the Olympus BX51 microscope by a single mode optical fiber. The laser was focused to 1 um in diameter through a 100X object len (NA = 0.8). The microfibers of **1** and **2** were dispersed in ethanol and then deposited onto glass. Single wire with width of about 1 μm was excited under dark field with laser spot through microscope and recorded with a DVC-1412 M CCD camera. The data were analyzed with Image J software and the relative gray values of $I(X)/I_o$ were plotted against distance X to obtain the optical loss value α.

Compound **6** was prepared according to Babudri et al.[36] and compound **11**−**14** was prepared according to Foster et al.[37]

General Procedure for Compounds 1−**5.** A mixture of diketone (0.2 mmol), benzene-1,2,4,5-tetraamine tetrachloride (0.1 mmol), and sodium acetate (0.4 mmol) in ethanol (10 mL) were refluxed overnight under nitrogen. Ethanol was removed from the resulting mixture under reduced pressure, and the residue was redissolved in dichloromethane. After washing by water for two times, the combined organic phase was dried and the solvent was removed under reduced pressure. The residue was further purified by column chromatography (silica gel, petroleum ether: dichloromethane = 3: 1 to 1: 1) to give the desired products.

2,3,7,8-Tetrakis(4-(dodecyloxy)phenyl)pyrazino[2,3-g]quinoxaline (1). Yield: 58%, as yellow solid. ^{1}H NMR ($CDCl_3$, 300 MHz, ppm): δ 8.88 (2H, s), 7.57−7.60 (8H, d, J = 9.0 Hz), 6.88−6.91 (8H, d, J = 9.0 Hz), 3.98−4.02 (8H, t, J = 6.6 Hz), 1.76−1.85 (8H, m), 1.24−1.34 (72H, m), 0.86−0.91 (12H, t, J = 6.6 Hz). ^{13}C NMR ($CDCl_3$, 50 MHz, ppm): δ = 159.8, 154.2, 139.9, 131.4−130.9., 113.9−114.1, 67.7, 31.6, 29.8−28.9, 25.7, 22.4, 13.8. Elemental anal. Calcd for $C_{82}H_{118}N_4O_4$: C, 80.47; H, 9.72; N, 4.58. Found: C, 79.86; H, 9.58; N, 4.63. MALDI-ICR-FTMS m/z: calcd, 1223.923; found, 1223.928 [MH^+].

(36) Babudri, F.; Fiandanese, V.; Marchese, G.; Punzi, A. *Tetrahedron Lett*. **1995**, *36*, 7305–7408.
(37) Foster, E. J.; Babuin, J.; Ngugen, N.; Williams, V. E. *Chem. Commun*. **2004**, 2052–2053.

2,3,7,8-Tetrakis(5-dodecylthiophen-2-yl)pyrazino[2,3-g]quinoxaline (2). Yield: 70%, as reddish orange solid. ^{1}H NMR ($CDCl_3$, 300 MHz, ppm): δ 8.63 (2H, s), 7.24−7.25 (4H, d, J = 3.6 Hz), 6.72−6.73 (4H, d, J = 3.6 Hz), 2.86−2.91 (8H, t, J = 7.5 Hz), 1.73−1.78 (8H, m), 1.27−1.41 (72H, m), 0.86−0.90 (12H, t, J = 6.6 Hz). ^{13}C NMR ($CDCl_3$, 50 MHz, ppm): δ = 151.0, 147.7, 139.4, 138.7, 130.1, 124.5, 31.6, 31.3, 30.1, 29.6−28.9, 22.4, 13.8. Elemental anal. Calcd for $C_{74}H_{110}N_4S_4$: C, 75.07; H, 9.36; N, 4.73; S, 10.83. Found: C, 74.85; H, 9.37; N, 4.66; S, 10.56. MALDI-ICR-FTMS m/z: calcd, 1183.769; found, 1183.767 [MH^+].

2,3-Bis(4-(dodecyloxy)phenyl)-7,8-bis(5-dodecylthiophen-2-yl)-pyrazino[2,3-g]quinoxaline (3). Yield: 13%, as yellowish orange solid. ^{1}H NMR ($CDCl_3$, 300 MHz, ppm): δ 8.75 (2H, s), 7.55−7.58 (4 H, d, J = 8.7 Hz), 7.23−7.24 (2H, d, J = 3.0 Hz), 6.87−6.90 (4H, d, J = 8.7 Hz), 6.73−6.74 (2H, d, J = 3.6 Hz), 3.98−4.02 (4H, t, J = 6.3 Hz), 2.86−2.88 (4H, t, J = 7.8 Hz), 1.73−1.80 (8H, m), 1.21−1.44 (72H, m), 0.86−0.96 (12H, t, J = 6.6 Hz). ^{13}C NMR ($CDCl_3$, 50 MHz, ppm): δ = 159.9, 150.9, 130.9−131.1, 130.1, 127.1, 124.54, 113.9−114.0, 110.0, 67.8, 31.2−31.6, 30.1, 29.3−28.2, 25.7, 22.4, 13.8. Elemental anal. Calcd for $C_{78}H_{114}N_4O_2S_2$: C, 77.82; H, 9.54; N, 4.65; S, 5.33. Found: C, 77.57; H, 9.38; N, 4.54; S, 5.39. MALDI-ICR-FTMS m/z: valcd, 1203.846; found, 1203.850 [MH^+].

2,7-Bis(3,4-bis(dodecyloxy)phenyl)-3,8-diphenylpyrazino[2,3-g]-quinoxaline (4). Yield: 69%. ^{1}H NMR ($CDCl_3$, 300 MHz, ppm): δ 8.98 (2H, s), 7.63−7.66 (4H, m), 7.41−7.43 (6H, m), 7.27−7.30 (2H, dd, J_1 = 1.8 Hz, J_2 = 8.1 Hz), 7.05−7.07 (2H, d, J = 1.8 Hz), 6.88−6.91 (2H, d, J = 8.4 Hz), 4.02−4.07 (4H, t, J = 6.6 Hz), 3.75−3.79 (4H, t, J = 6.6 Hz), 1.83−1.88 (4H, m), 1.70−1.75 (4H, m), 1.22−1.49 (72H, m), 0.87−0.91 (12H, t, J = 6.9 Hz). ^{13}C NMR ($CDCl_3$, 50 MHz, ppm): δ = 155.4−155.5, 154.8, 150.5, 148.5, 143.7, 140.7−140.4, 139.5, 131.0, 129.9, 129.4, 128.5, 123.5, 116.9, 115.5, 97.6, 95.5, 88.7, 69.2, 69.1, 44.2−43.7, 32.4−32.1, 29.9−29.1, 26.2, 22.9, 14.4. Elemental anal. Calcd for $C_{82}H_{118}N_4O_4$: C, 80.47; H, 9.72; N, 4.58. Found: C, 80.46; H, 9.70; N, 4.56. MALDI-ICR-FTMS m/z: calcd, 1223.923; found, 1223.917 [MH^+].

2,3,7,8-Tetrakis(4-methylphenyl)pyrazino[2,3-g]quinoxaline (5). ^{1}H NMR ($CDCl_3$, 300 MHz, ppm): δ 8.89 (2H, s, Ar−H), 7.59−7.61 (8 H, d, Ar−H, J = 6.6 Hz), 6.91−6.93 (8 H, d, Ar−H, J = 7.5 Hz), 3.86 (12 H, s, CH_3). ESI-ICR-FTMS m/z: calcd, 607.234; found, 607.234 [MH^+].

1,2-Bis(5-dodecylthiophen-2-yl)ethane-1,2-dione (6). Yield: 40%, a yellow solid. ^{1}H NMR ($CDCl_3$, 300 MHz, ppm): δ 7.87−7.88 (2H, d, J = 3.9 Hz), 6.89−6.90 (2H, d, J = 3.9 Hz), 2.87−2.92 (4H, t, J = 7.5 Hz), 1.71−1.75 (4H, m), 1.27−1.34 (36H, m), 0.87−0.91 (6H, t, J = 6.6 Hz). Elemental anal. Calcd for $C_{34}H_{54}O_2S_2$: C, 73.06; H, 9.74; S, 11.47. Found: C, 73.34; H, 9.88; S, 10.86. ESI-ICR-FTMS m/z: calcd, 559.364; found, 559.364 [MH^+].

1-(3,4-Bis(dodecyloxy)phenyl)-2-phenylethane-1,2-dione (14). Yield: 78%, a white solid. ^{1}H NMR ($CDCl_3$, 300 MHz, ppm): δ 7.95−7.98 (2H, m), 7.60−7.63 (1H, m), 7.57−7.58 (1H, d, J = 2.1 Hz), 7.48−7.53 (2H, d, J = 8.1 Hz), 7.40−7.42 (1H, dd, J_1 = 1.8 Hz, J_2 = 8.1 Hz), 7.26−7.27(1H, d, J = 2.7 Hz), 6.84−6.87 (1H, d, J = 8.7 Hz), 4.04−4.08 (4H, t, J = 5.4 Hz), 1.83−1.88 (4H, m), 1.30−1.47 (36H, m), 0.85−0.90 (6H, t, J = 6.0 Hz). Elemental anal. Calcd for $C_{38}H_{58}O_4$: C, 78.85; H, 10.10. Found: C, 78.87; H, 10.03. ESI-ICR-FTMS m/z: calcd, 579.441; found, 579.440 [MH^+].

Acknowledgment. This work was supported by the Major State Basic Research Development Program (2006CB921602 and 2009CB623601) from the Ministry of Science and Technology, and National Natural Science Foundation of China. We thank Dr. Haibin Song for single crystal elucidation and Lin Ding for SEM experiments.

Note Added after ASAP Publication. There was a spelling error in an author's name in the version published ASAP May 21, 2010; the corrected version was published May 25, 2010.

Supporting Information Available: Data of calculated energy level of molecular orbitals, UV−vis and fluorescence spectra in different solvent and in solid, DSC spectra, ^{1}HNMR spectra, and ^{13}CNMR spectra (PDF); information of single-crystal structure (CIF file). This material is available free of charge via the Internet at http://pubs.acs.org.